Journal of Nuclear Materials 529 (2020) 151955

Contents lists available at ScienceDirect

Journal of Nuclear Materials

journal homepage: www.elsevier.com/locate/jnucmat

Ion irradiation response and mechanical behavior of reduced activity high entropy alloy

Maryam Sadeghilaridjani [a], Aditya Ayyagari [a], Saideep Muskeri [a], Vahid Hasannaeimi [a], Riyadh Salloom [a], Wei-Ying Chen [b], Sundeep Mukherjee [a, *]

[a] Department of Materials Science and Engineering, University of North Texas, Denton, TX, 76203, USA
[b] Argonne National Laboratory, Lemnot, IL, 60439, USA

ARTICLE INFO

Article history:
Received 10 October 2019
Received in revised form
27 November 2019
Accepted 10 December 2019
Available online 11 December 2019

Keywords:
High entropy alloy
Ion irradiation
Nano-indentation
Micro-pillar compression
Self-healing

ABSTRACT

Refractory alloys consisting of reduced activity elements are attractive for nuclear applications to allow safe post-service recycling and meet fusion reactor requirements. Here, ion irradiation response was studied for a newly developed refractory high entropy alloy, HfTaTiVZr, with low activation constituent elements. Ion irradiation led to around 20% hardening for the high entropy alloy compared to 50% hardening for stainless steel under identical conditions. Superior irradiation resistance of the concentrated alloy was explained by the reduced mobility of point defects and self-healing ability.

1. Introduction

Several critical attributes need to be simultaneously satisfied for material selection in advanced nuclear applications including irradiation resistance, high temperature hardness, creep resistance, hot corrosion resistance, dimensional stability, and resistance to swelling, flaking, and thermal fatigue [1,2]. The continued challenge in developing materials that have exceptional multi-tier properties, which exceed the limits of current nuclear materials, has deemed materials development for advanced reactor technologies as one of the long-standing issues faced by the engineering community [2,3]. Novel technologies including advanced coatings, ceramic-composites, and refractory alloys are being actively explored to address these challenges [1,4,5]. One such paradigm in material design strategy is the concept of multi-principal element alloys, where five or more elements are mixed in equal or nearly equal proportions commonly referred to as high entropy alloys (HEAs) or more generically as complex concentrated alloys (CCAs) [6,7]. Although composed of multiple elements, the resulting microstructure consists of a single-phase in HEAs or multiple solid solution phase mixtures in CCAs with good thermal stability [6,7]. High configurational entropy of mixing in these systems suppresses intermetallic formation in many cases and results in high degree of lattice strain from the presence of different sized atoms in the unit cell [6,7]. There are several reports on the irradiation behavior of high entropy alloys [8–18]. However, a significant drawback in most of the reported alloys is the rather long time it would take to reach "hands-on" level to be safely recycled. Although there is no radioactivity in the fusion reactor core, structural materials in the vicinity gain radioactivity from prolonged exposure to high-energy neutrons from the plasma [19]. Therefore, reduced activation is critical for safe recycling of these materials within a relatively short period after decommissioning of the reactor as well as offering low thermal neutron absorption cross-section [20]. Development of low activity high entropy alloys has the potential to significantly advance next-generation fission and fusion reactors and have a profoundly positive environmental impact [21,22].

Here, we report on the irradiation response and associated mechanical behavior of a refractory high entropy alloy, HfTaTiVZr. All constituent elements of this alloy belong to the 4-5-6 refractory alloy group and have inherently low activity with shorter "hands-on" time [21,22] compared to compositions based on elements such as Mo, Nb and Ni. The alloy was developed using theoretical

* Corresponding author.
E-mail address: sundeep.mukherjee@unt.edu (S. Mukherjee).

https://doi.org/10.1016/j.jnucmat.2019.151955
0022-3115/

modelling via Ab Initio Molecular Dynamics (AIMD) for high entropy phase formation [21] and showed a compressive yield strength of 1 GPa at room temperature and good creep resistance [23]. In this paper, we report on the irradiation response of the alloy after exposing to 4.4 MeV high energy Ni^{2+} ions. The irradiated samples were characterized using nano-indentation, micro-pillar compression, and transmission electron microscopy to understand the associated change in structure and mechanical behavior. The results for the high entropy alloy were compared with 304 stainless steel (SS304) under identical heavy ion exposure conditions, as a currently used benchmark material in nuclear applications.

2. Experimental

An alloy with nominal composition of HfTaTiVZr (equimolar proportion of elements) was prepared by arc-melting in a Ti-gettered argon atmosphere using constituent elements with purity greater than 99.99%. To ensure chemical homogeneity, the sample was flipped and remelted at least four times. The bulk HfTaTiVZr alloy and SS304 were cut and mechanically polished with silicon carbide papers and diamond polishing paste to mirror finish for microstructure characterization, ion irradiation and nano-mechanical tests. The structure of the alloys was characterized by Rigaku III Ultima X-ray diffractometer (XRD, Rigaku Corporation, Tokyo, Japan) using Cu-Kα radiation with wavelength of 1.54 Å. Scanning electron microscopy (SEM) using FEI Quanta ESEM (FEI Company, Hillsboro, OR, USA) with in-built energy dispersive spectroscopy (EDS) and electron backscatter diffraction (EBSD) were done to analyze the microstructure and grain size of the samples.

The prepared samples were irradiated at room temperature with 4.4 MeV high energy Ni^{2+} ions with a fluence of 1.08×10^{17} ions cm^{-2} at the Michigan Ion Beam Laboratory. The temperature was monitored by a thermal imager. The irradiated alloys were analyzed by transmission electron microscopy (TEM) on FEI Tecnai F20 operating at 200 kV. Samples for cross-section transmission electron microscopy were prepared using FEI Nova NanoLab 200 focused ion beam SEM (FIB-SEM). The projected range and displacement damage profiles were calculated using the Stopping and Range of Ions in Matter (SRIM) software package. The SRIM calculation was done in the full damage cascade mode and 25 eV energy was used.

To assess the surface mechanical properties of the alloys after irradiation, nano-indentation was done using a TI-Premier Triboindenter (Bruker, Minneapolis, MN, USA) with Berkovich diamond tip. High temperature nano-indentation was done in an $Ar + H_2$ gas environment to avoid surface oxidation. The samples were indented along the direction of ion irradiation. Hardness was measured according to the Oliver and Pharr method [24] as a function of depth from 100 nm to 2500 nm in displacement control mode with a high load transducer (maximum load of 10 N). A minimum of ten indents were made for each depth with 100 μm spacing between two indents to avoid any overlap of their plastic zones. For micro-pillar compression test, pillars ~1 μm in diameter and ~1.5 μm in height were fabricated on the surface of the irradiated and un-irradiated samples (along the irradiation direction) using FEI Nova NanoLab 200 FIB-SEM in several steps using Ga ion beam with current ranging from 5 nA to 10 pA and energy of 30 keV. The taper angle measured for each pillar was less than 2°. Three to five pillars were fabricated for each condition to get an average value for the different crystallographic orientations. In-situ micro-pillar compression tests were performed using PI88 SEM Picoindenter (Bruker, Minneapolis, MN, USA) equipped with a 5 μm flat punch diamond tip at a strain rate of 8×10^{-3} s^{-1} in displacement control mode. The load-displacement data were converted to engineering stress-strain values for further analysis.

3. Results and discussion

Fig. 1 (a) shows the relatively short period of time required for refractory elements found in the current HEA (i.e., Hf, Ta, Ti, V, and Zr) to reach "hands-on" level after irradiation [25]. Nano-indentation hardness of HfTaTiVZr alloy and SS304 as a benchmark material is shown in Fig. 1 (b) as a function of temperature. HfTaTiVZr showed nearly two times higher hardness compared with SS304 at room temperature and the change in hardness of HfTaTiVZr from room temperature to 723 K was not significant. These results suggest that the current HEA may be a good candidate for nuclear and high temperature applications compared with conventional alloys like stainless steel. Fig. 1 (c) shows the X-ray diffraction pattern of the as-cast HEA as well as after annealing at 723 K for 2 h indicating its single-phase body centered cubic (BCC) structure without any secondary phases. The HfTaTiVZr high entropy alloy annealed at 723 K for 2 h showed identical structure and diffraction peak positions as the cast alloy supporting its good microstructural stability. TEM characterization of the as-cast sample was done and inset of Fig. 1 (c) shows the selected area diffraction (SAD) pattern along [011] zone axis further confirming the single-phase BCC structure. SEM image and EDS mapping of the alloy are shown in Fig. 1 (d) and 1 (e), respectively, confirming homogeneous distribution of elements with no segregation or secondary phases. The HfTaTiVZr high entropy alloy showed equiaxed microstructure with average grain size ~150 μm as observed from the EBSD image in Fig. 1 (f).

Irradiation damage quantified in terms of displacements per atom (dpa) versus depth profile for HfTaTiVZr HEA was calculated using SRIM as shown in Fig. 2 (a). Ni ion concentration as a function of depth is also shown in Fig. 2 (a) indicating maximum Ni concentration of 0.02 at% at depth of ~2500 nm. Peak damage was ~40 dpa at a depth of approximately 2000 nm from the surface. Fig. 2 (b) and 2 (c) show the cross-sectional TEM image of irradiated HEA with selected area diffraction (SAD) patterns along the [102] zone axis at different depths below the surface: (1) 500 nm, (2) 1000 nm, (3) 1500 nm, (4) 2000 nm, and (5) 2500 nm. SAD patterns show irradiation-induced amorphization with varying degree through the ion projected range. Areas 1 and 2 with lower irradiation dosage (~20–25 dpa) remained relatively unchanged. On the other hand, areas 3 and 4 at the peak damage level (~35–40 dpa) were found to have a mixture of amorphous and crystalline phases. Area 5 also showed partial amorphization. Disordering and partial amorphization has been reported for several materials after exposure to high energy ion irradiation [26]. High-entropy nitride coatings (TiHfZrNbVTa)N have recently been reported to undergo change to amorphous structure after heavy ion implantation of Au^- and N^+ [27–29]. The current HEA was resistant to amorphization up to 30 dpa at 298 K. In contrast, most structural alloys showed significantly higher damage level at lower dosage [26,30,31]. Intermetallic compounds amorphized usually at 0.1 to 0.5 dpa [30] and the structure of nuclear grade steels and refractory metals changed after 1 to 3 dpa irradiation at room temperature [26,31]. Materials with a natural tendency to accommodate lattice disorder typically show better irradiation resistance [32]. In these alloys, dislocation nucleation is relatively more difficult and the recrystallized state shows low defect density [11,33,34]. Previous studies on $Al_{1.5}CoCrFeNi$ [14] and Hf-Nb-Zr [17] HEAs demonstrated no obvious structural change, voids, swelling, and segregation after irradiation even at elevated temperatures and doses higher than 40 dpa. CrFeMnNi HEA showed less radiation damage compared to Cr-Ni and Cr-Mn austenitic steels [12].

As irradiation depth is typically limited to few micrometers from

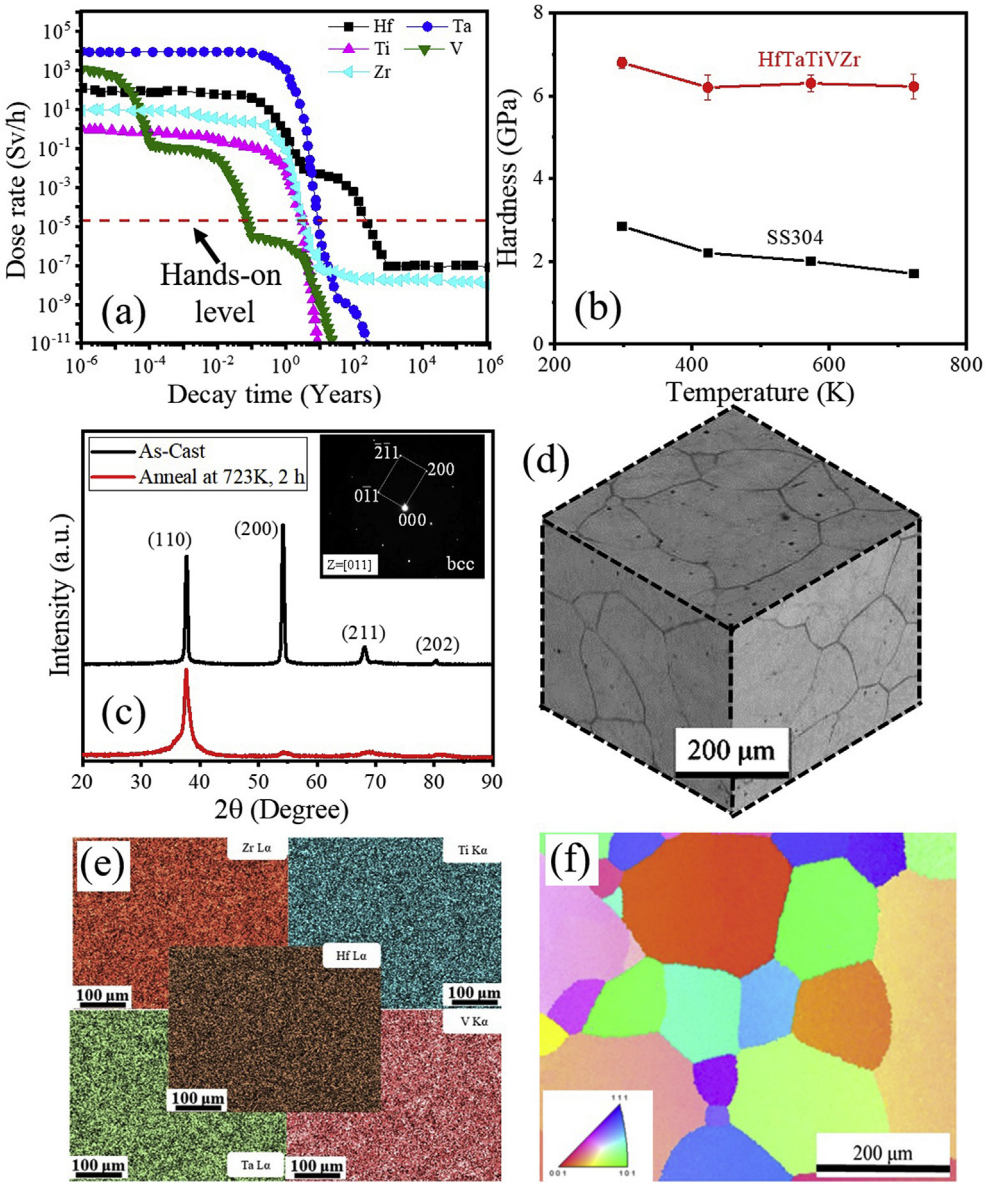

Fig. 1. (a) Time in years required for Hf, Ta, Ti, V, and Zr to reach "hands-on" level after exposure [25]; (b) hardness as a function of temperature for HfTaTiVZr high entropy alloy and SS304; (c) X-ray diffraction of as-cast and annealed HfTaTiVZr high entropy alloy indicating single-phase BCC crystal structure with the inset showing selected area diffraction pattern along [011] zone axis; (d) scanning electron microscopy showing single-phase microstructure and equiaxed grains for the HEA; (e) energy dispersive spectroscopy showing homogeneous distribution of elements in the HEA with no secondary phases or segregation; (f) electron backscatter diffraction (EBSD) image showing equiaxed grains with an average grain size of ~150 μm.

the surface, nano-indentation has been utilized to characterize the change in mechanical behavior of irradiated samples [12,35,36]. However, significant care should be taken for interpretation of the data due to issues related to indentation size effect or dose range effect [37]. Nano-indentation was done in un-irradiated and irradiated regions of the HfTaTiVZr HEA and SS304. The obtained hardness as a function of indentation depth from 100 nm to 2500 nm is shown in Fig. 3 (a) and 3 (b). Each data point in Fig. 3 represents the average value of ten indents. The hardness for both the alloys in irradiated and un-irradiated conditions was found to decrease with increasing depth. This was attributed to strain gradient plasticity to accommodate the shape of the Berkovich indenter [38,39]. Both the HEA and SS304 showed hardening after irradiation for the entire depth range of nano-indentation measurement. However, from Fig. 3 (a) and 3 (b) it is clear that the magnitude of hardening was significantly lesser for the HEA compared with SS304. The insets show hardness values for the depth range of 1500 nm–2000 nm with the HEA showing ~13% hardening compared to ~50% for SS304. The hardness of the irradiated sample did not approach that of the un-irradiated one at maximum depth because each indent sampled the entire region from the surface to the depth of indentation [40]. The difference in hardness from various crystallographic orientations is likely to be small compared to that caused by irradiation [41]. In addition, the indented area in the current study covered several grains. Therefore, the measured hardness is likely the average of several different crystallographic orientations.

To further characterize the change in mechanical behavior after irradiation, micro-pillar compression tests were performed. Pre- and post-compression images of representative pillars from each

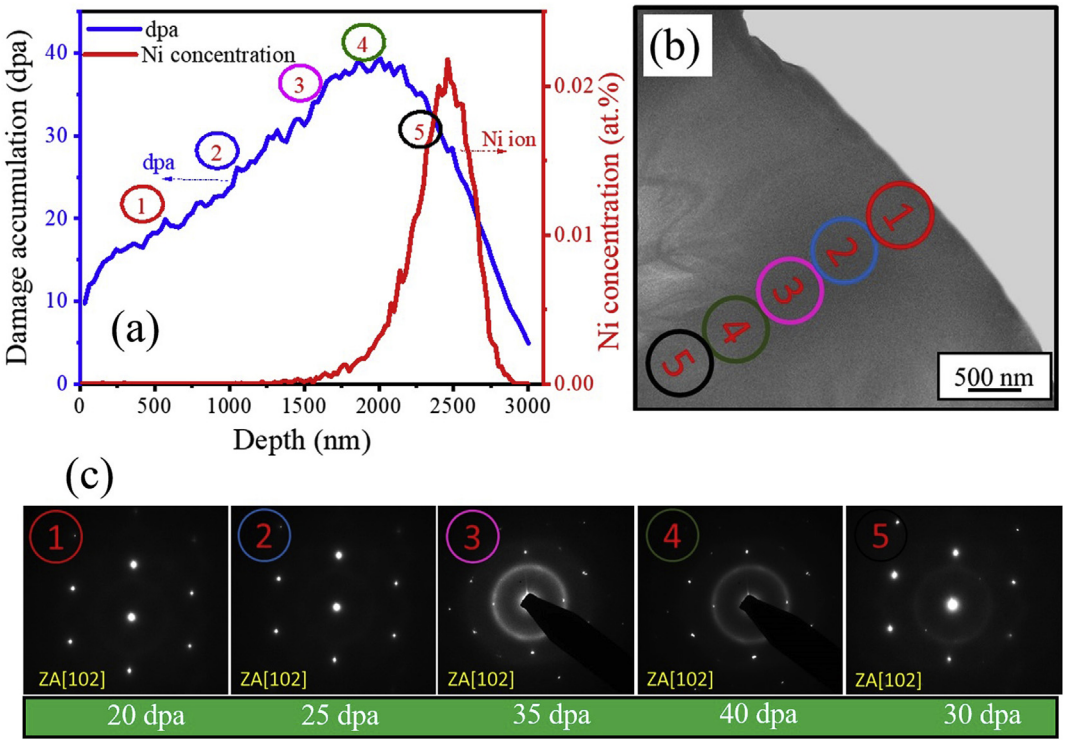

Fig. 2. (a) Irradiation induced damage in HfTaTiVZr alloy calculated using SRIM showing peak damage of 40 dpa at around 2000 nm depth from surface along with the Ni ion concentration as a function of depth showing maximum Ni concentration of 0.02 at% at depth of ~2500 nm; (b) cross-sectional transmission electron microscopy and (c) selected area diffraction patterns of irradiated HfTaTiVZr alloy at different depth from surface; selected areas are shown with numbers from ① to ⑤. Partial amorphization is seen for regions with maximum dpa.

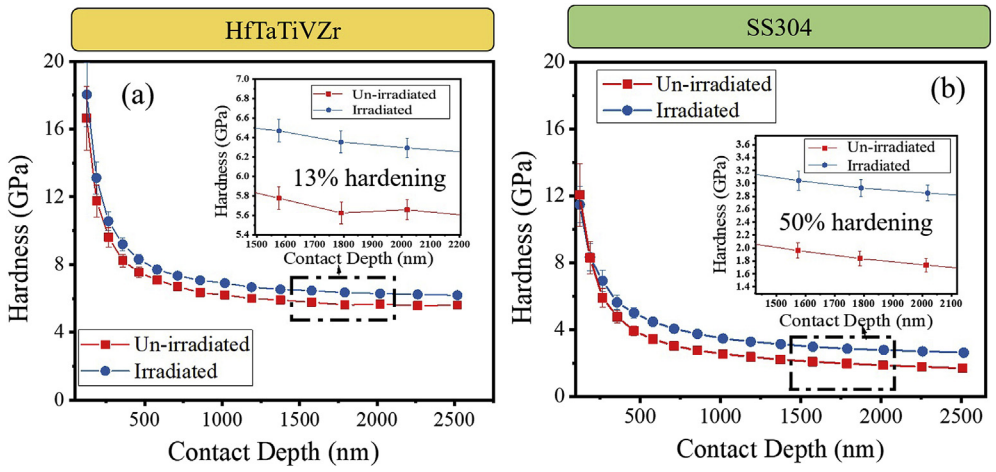

Fig. 3. Hardness versus depth for irradiated and un-irradiated samples of (a) HfTaTiVZr high entropy alloy and (b) 304 stainless steel (SS304) showing hardening of both alloys after irradiation but to different degrees: 13% hardening for high entropy alloy and 50% hardening for SS304 in the depth range of 1500–2000 nm.

alloy after irradiation are shown in Fig. 4 (a)-4 (d). Fig. 4 (a) and 4 (c) show SEM images of pristine and deformed micro-pillar for HfTaTiVZr alloy, respectively. SEM image in Fig. 4 (b) and 4 (d) show the representative un-deformed and compressed micro-pillar for SS304. For both the alloys, the compressed pillars underwent plastic deformation via multiple slip planes initiated near the top surface close to the indenter and propagated downward. The pillars fabricated on un-irradiated samples showed similar failure mode and are not included. Fig. 4 (e) and 4 (f) show the engineering stress-strain curves obtained from micro-pillar compression of un-irradiated and irradiated HEA and SS304 samples, respectively. Three pillars were tested for each condition to obtain the standard deviation. The yield strength in all cases was obtained using 0.2% strain offset and is shown for each pillar. Both alloys showed hardening after irradiation. For the HEA, average yield strength increased from 1074 MPa in the un-irradiated state to 1381 MPa after ion irradiation (28% hardening). The average yield strength for SS304 increased from 484 MPa to 745 MPa (54% hardening). Since the level of damage varies through the height of the micro-pillar, the obtained irradiation-induced hardening is the response for a range of dpa. The magnitude of hardening for SS304 was almost two times that of the HEA in agreement with nano-indentation

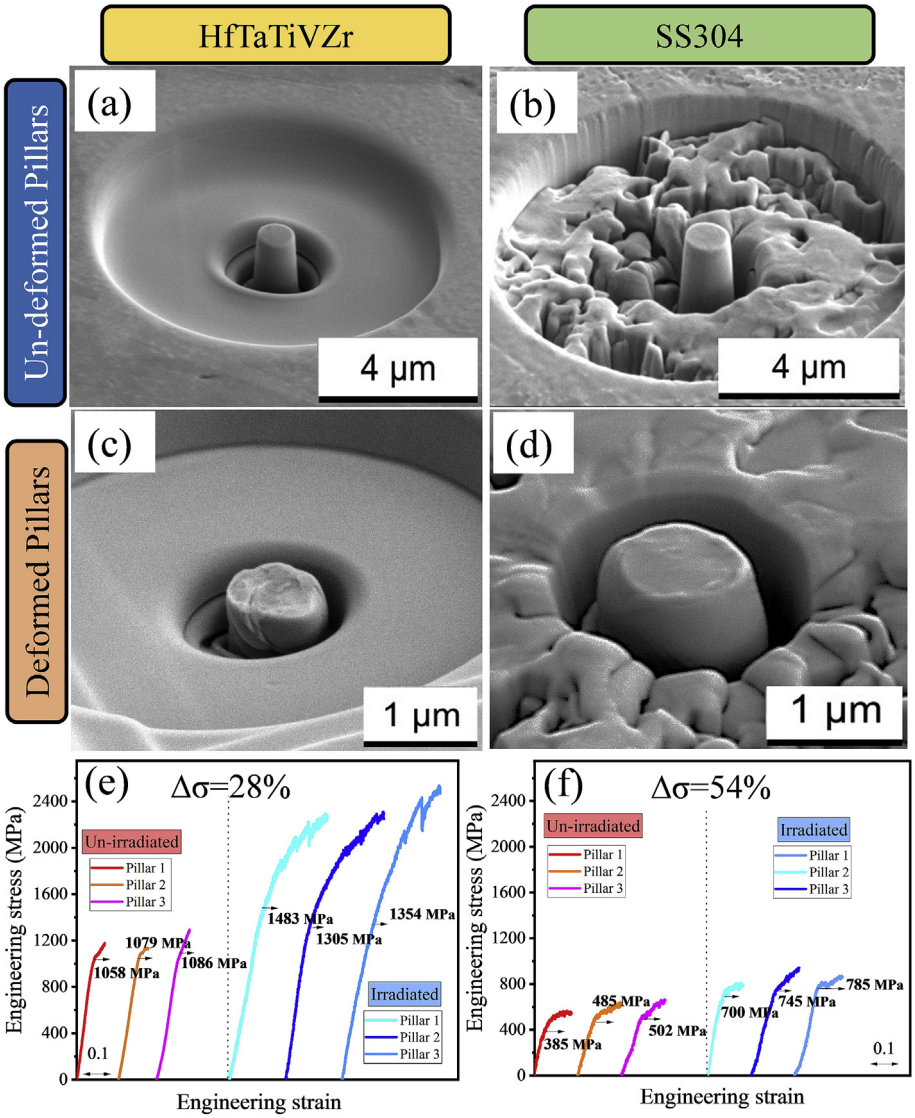

Fig. 4. SEM image of un-deformed micro-pillars for (a) irradiated HfTaTiVZr HEA and (b) irradiated SS304; SEM image of micro-pillars after compression test for (c) irradiated HfTaTiVZr HEA and (d) irradiated SS304. Engineering stress-strain response of un-irradiated and irradiated samples after compression test with strain rate of 8×10^{-3} s^{-1} for (e) HfTaTiVZr HEA, and (f) SS304. Yield strength for each pillar at 0.2% offset strain is shown in the figures by arrows. There was 28% increase in average yield strength for HfTaTiVZr HEA after irradiation and 54% increase for SS304.

results. Increase in hardness and yield strength after irradiation has been reported previously for SS304 [35], HT-9 [36], high entropy alloys [8,18], and bulk metallic glasses [42,43]. Hardening of irradiated alloys has been explained based on hindrance in dislocation motion due to defects such as precipitates, loops, and voids [8,44]. Accumulation of these defects cause structural damage and degrade the performance of materials over time [45].

The magnitude of hardening for ion-irradiated high entropy alloy was significantly smaller compared to SS304. This may be due to different type and density of defects generated in the HEA after irradiation compared with steel [12]. In both the cases, ion radiation displaces the atoms from their position and leads to vacancy and interstitial defects. Point defects in HEAs have high formation energy and atomic-level stress [46], which make them unstable and prone to annihilation. This process is expected to leave significantly lower defect density in HEAs compared to the steel. Recombination of vacancies and interstitials was found to be the dominant recovery process in HEAs, which has been attributed to increased compositional complexity and atomic size mismatch between the constituent principal elements. Radiation damage and void swelling decrease with increase in compositional complexity [13]. In fact, one of the approaches proposed for design of radiation-resistant materials is immobilization of point defects [18,47]. Each atom in the HEA is surrounded by different neighboring atoms with varying bond configurations and lattice potential energies. Diffusion of an atom from one position to another with a different lattice potential energy may not be energetically favorable, thereby reducing the effective interstitial and vacancy mobility. Formation and growth of vacancy clusters and dislocation loops are hindered and recombination of vacancy-interstitial is facilitated [10,12,16,48]. Molecular dynamics (MD) simulations showed that the mobility of defects is lower in multi-component solid solutions compared to that in pure metals [49]. Most of the irradiation-induced vacancies in the current HEA were likely annihilated by interstitials, grain boundaries (GBs), and interfaces resulting in a self-healing process [11]. This explains its higher irradiation resistance compared to conventional nuclear materials such as SS304. Because of distorted lattice in HEAs and higher equilibrium vacancy

concentration, the incident heavy ions are captured by vacancies leading to some degree of self-healing [50].

4. Conclusion

In summary, the irradiation behavior of a refractory high entropy alloy, HfTaTiVZr, with reduced activity constituent elements was studied and compared with 304 stainless steel. Irradiation-induced structural change and amorphization was found to be relatively limited in the HEA, which was attributed to its distorted lattice and high atomic level strain. Increase in hardness and yield strength for the HEA was ~20% and for SS304 was ~50% under identical irradiation conditions. Better irradiation resistance of the HEA was attributed to its self-healing ability. Sluggish diffusion of atoms in the HEA reduced effective interstitial and vacancy mobility and limited irradiation induced damage.

Declaration of competing interest

The authors declare that they have no known competing financial interests or personal relationships that could have appeared to influence the work reported in this paper.

CRediT authorship contribution statement

Maryam Sadeghilaridjani: Methodology, Formal analysis, Investigation, Writing - original draft. **Aditya Ayyagari:** Methodology, Investigation, Writing - original draft. **Saideep Muskeri:** Formal analysis, Investigation, Writing - original draft. **Vahid Hasannaeimi:** Formal analysis, Investigation, Writing - original draft. **Riyadh Salloom:** Investigation, Writing - original draft. **Wei-Ying Chen:** Validation, Writing - review & editing. **Sundeep Mukherjee:** Conceptualization, Validation, Writing - review & editing, Supervision.

Acknowledgements

This work was partly funded by U.S. Department of Energy under an SBIR/STTR sub-contract, DE-SC0017138. The authors also thank Dr. Ovidiu Toader at Michigan Ion Beam Laboratory (MIBL) for heavy ion irradiation of the samples and helpful discussion.

References

[1] B. Raj, M. Vijayalakshmi, P.R.V. Rao, K.B.S. Rao, Challenge in materials research for sustainable nuclear energy, MRS Bull. 33 (2008) 327–337.
[2] S.J. Zinkle, J.T. Busby, Structural materials for fission and fusion energy, Mater. Today 12 (2009) 12–19.
[3] R.W. Grimes, R.J.M. Konings, L. Edwards, Greater tolerance for nuclear materials, Nat. Mater. 7 (2008) 683–685.
[4] E. Alat, A.T. Motta, R.J. Comstock, J.M. Partezana, D.E. Wolfe, Multilayer (TiN, TiAlN) ceramic coatings for nuclear fuel cladding, J. Nucl. Mater. 478 (2016) 236–244.
[5] Y. Wu, FDS team, Fusion-based hydrogen production reactor and its material selection, J. Nucl. Mater. 386–388 (2009) 122–126.
[6] D.B. Miracle, O.N. Senkov, A critical review of high entropy alloys and related concepts, Acta Mater. 122 (2017) 448–511.
[7] Y. Zhang, T.T. Zuo, Z. Tang, M.C. Gao, K.A. Dahmen, P.K. Liaw, Z.P. Lu, Microstructures and properties of high-entropy alloys, Prog. Mater. Sci. 61 (2014) 1–93.
[8] S.-q. Xia, Z. Wang, T.-f. Yang, Y. Zhang, Irradiation behavior in high entropy alloys, J. Iron Steel Res. Int. 22 (2015) 879–884.
[9] Y. Lu, H. Huang, X. Gao, C. Ren, J. Gao, H. Zhang, S. Zheng, Q. Jin, Y. Zhao, C. Lu, T. Wang, T. Li, A promising new class of irradiation tolerant materials: $Ti_2ZrHfV_{0.5}Mo_{0.2}$ high-entropy alloy, J. Mater. Sci. Technol. 35 (2019) 369–373.
[10] T.-n. Yang, C. Lu, G. Velisa, K. Jin, P. Xiu, Y. Zhang, H. Bei, L. Wang, Influence of irradiation temperature on void swelling in NiCoFeCrMn and NiCoFeCrPd, Scr. Mater. 158 (2019) 57–61.
[11] T. Egami, W. Guo, P.D. Rack, T. Nagase, Irradiation resistance of multicomponent alloys, Metall. Mater. Trans. A 45 (2014) 180–183.
[12] N.A.P.K. Kumar, C. Li, K.J. Leonard, H. Bei, S.J. Zinkle, Microstructural stability and mechanical behavior of FeNiMnCr high entropy alloy under ion irradiation, Acta Mater. 113 (2016) 230–244.
[13] C. Lu, L. Niu, N. Chen, K. Jin, T. Yang, P. Xiu, Y. Zhang, F. Gao, H. Bei, S. Shi, M.-R. He, I.M. Robertson, W.J. Weber, L. Wang, Enhancing radiation tolerance by controlling defect mobility and migration pathway in multicomponent single-phase alloys, Nat. Commun. 7 (2016), 13564.
[14] S.Q. Xia, X. Yang, T.F. Yang, S. Liu, Y. Zhang, Irradiation resistance in AlxCoCrFeNi high entropy alloys, JOM 67 (2015) 2340–2344, https://doi.org/10.1007/s11837-015-1568-4.
[15] O. El-Atwani, N. Li, M. Li, A. Devaraj, J.K.S. Baldwin, M.M. Schneider, D. Sobieraj, J.S. Wrobel, D. Nguyen-Manh, S.A. Maloy, E. Martinez, Outstanding radiation resistance of tungsten-based high entropy alloys, Sci. Adv. 5 (2019) 1–9.
[16] S. Xia, M.C. Gao, T. Yang, P.K. Liaw, Y. Zhang, Phase stability and microstructures of high entropy alloys ion irradiated to high doses, J. Nucl. Mater. 480 (2016) 100–108.
[17] T. Nagase, S. Anada, P.D. Rack, J.H. Noh, H. Yasuda, H. Mori, T. Egami, Electron-irradiation-induced structural change in Zr-Hf-Nb alloy, Intermetallics 26 (2012) 122–130.
[18] W.-Y. Chen, X. Liu, Y. Chen, J.-W. Yeh, K.-K. Tseng, K. Natesan, Irradiation effects in high entropy alloys and 316H stainless steel at 300 °C, J. Nucl. Mater. 510 (2018) 421–430.
[19] M. Gorley, Critical assessment 12: prospects for reduced activation steel for fusion plant, Mater. Sci. Technol. 31 (2015) 975–980.
[20] P.J. Maziasz, R.L. Klueh, Precipitation Sensitivity to Alloy Composition in Fe–Cr–Mn Austenitic Steels Developed for Reduced Activation for Fusion Application, Reduced Activation Materials for Fusion Reactors, ASTM International, 1990.
[21] A. Ayyagari, R. Salloom, S. Muskeri, S. Mukherjee, Low activation high entropy alloys for next generation nuclear applications, Materialia 4 (2018) 99–103.
[22] A. Kareer, J.C. Waite, B. Li, A. Couet, D.E.J. Armstrong, A.J. Wilkinson, Short communication: 'Low activation, refractory, high entropy alloys for nuclear applications', J. Nucl. Mater. 526 (2019), 151744.
[23] M. Sadeghilaridjani, S. Muskeri, V. Hassannaeimi, M. Pole, S. Mukherjee, Strain rate sensitivity of a novel refractory high entropy alloy: intrinsic versus extrinsic effects, Mater. Sci. Eng. A 766 (2019), 138326.
[24] W.C. Oliver, G.M. Pharr, Measurement of hardness and elastic modulus by instrumented indentation: advances in understanding and refinements to methodology, J. Mater. Res. 19 (2004) 3–20.
[25] R.A. Forrest, A. Tabasso, C. Danani, S. Jakhar, A.K. Shaw, Handbook of Activation Data Calculated Using EASY-2007, EURATOM/UKAEA Fusion Association, 2009.
[26] C. Xu, W.-Y. Chen, Y. Chen, Y. Yang, Microstructural evolution of NF709 austenitic stainless steel under insitu ion irradiations at room temperature, 300, 400, 500 and 600 °C, J. Nucl. Mater. 509 (2018) 644–653.
[27] A.D. Pogrebnjak, O.V. Bondar, S.O. Borba, G. Abadias, P. Konarski, S.V. Plotnikov, V.M. Beresnev, L.G. Kassenova, P. Drodziel, Nanostructured multielement (TiHfZrNbVTa)N coatings before and after implantation of N^+ ions (10^{18} cm^{-2}): their structure and mechanical properties, Nucl. Instrum. Methods Phys. Res. Sect. B Beam Interact. Mater. Atoms 385 (2016) 74–83.
[28] A.D. Pogrebnjak, I.V. Yakushchenko, O.V. Bondar, V.M. Beresnev, K. Oyoshi, O.M. Ivasishin, H. Amekura, Y. Takeda, M. Opielak, C. Kozak, Irradiation resistance, microstructure and mechanical properties of nanostructured (TiZrHfVNbTa)N coatings, J. Alloy. Comp. 679 (2016) 155–163.
[29] A.D. Pogrebnjak, I.V. Yakushchenko, O.V. Sobol, V.M. Beresnev, A.I. Kupchishin, O.V. Bondar, M.A. Lisovenko, H. Amekura, K. Kono, K. Oyoshi, Y. Takeda, Influence of residual pressure and ion implantation on the structure, elemental composition, and properties of (TiZrAlYNb)N nitrides, Tech. Phys. 60 (2015) 1176–1183.
[30] D.T. Kulp, T. Egami, D.E. Luzzi, V. Vitek, Stress criteria for solid state amorphization, J. Non-Cryst. Solids 156–158 (1993) 510–513.
[31] O. El-Atwani, E. Esquivel, E. Aydogan, E. Martinez, J.K. Baldwin, M. Li, B.P. Uberuaga, S.A. Maloy, Unprecedented irradiation resistance of nanocrystalline tungsten with equiaxed nanocrystalline grains to dislocation loop accumulation, Acta Mater. 165 (2019) 118–128.
[32] K.E. Sickafus, R.W. Grimes, J.A. Valdez, A. Cleave, M. Tang, M. Ishimaru, S.M. Corish, C.R. Stanek, B.P. Uberuaga, Radiation-induced amorphization resistance and radiation tolerance in structurally related oxides, Nat. Mater. 6 (2007) 217–223.
[33] S. Mridha, M. Sadeghilaridjani, S. Mukherjee, Activation volume and energy for dislocation nucleation in multi-principal element alloys, Metals 9 (2019), 263.
[34] S. Mridha, S. Das, S. Aouadi, S. Mukherjee, R.S. Mishra, Nanomechanical behavior of CoCrFeMnNi high-entropy alloy, JOM 67 (2015) 2296–2302, https://doi.org/10.1007/s11837-015-1566-6.
[35] P. Hosemann, C. Shin, D. Kiener, Small scale mechanical testing of irradiated materials, J. Mater. Res. 30 (2015) 1231–1245.
[36] P. Hosemann, C. Vieh, R.R. Greco, S. Kabra, J.A. Valdez, M.J. Cappiello, S.A. Maloy, Nanoindentation on ion irradiated steels, J. Nucl. Mater. 389 (2009) 239–247.
[37] P. Hosemann, D. Kiener, Y. Wang, S.A. Maloy, Issues to consider using nano indentation on shallow ion beam irradiated materials, J. Nucl. Mater. 425 (2012) 136–139.
[38] M. Sadeghilaridjani, S. Mukherjee, Strain gradient plasticity in multiprincipal

element alloys, JOM 71 (2019) 3466–3472, https://doi.org/10.1007/s11837-019-03703-5.
[39] W.D. Nix, H. Gao, Indentation size effects in crystalline materials: a law for strain gradient plasticity, J. Mech. Phys. Solids 46 (1998) 411–425.
[40] D. Kiener, A.M. Minor, O. Anderoglu, Y. Wang, StA. Maloy, P. Hosemann, Application of small-scale testing for investigation of ion-beam-irradiated materials, J. Mater. Res. 27 (2012) 2724–2736.
[41] C.D. Hardie, S.G. Roberts, Nanoindentation of model Fe–Cr alloys with self-ion irradiation, J. Nucl. Mater. 433 (2013) 174–179.
[42] Y.Z. Yang, P.J. Tao, G.Q. Li, Z.X. Mu, Q. Ru, Z.W. Xie, X.C. Chen, Effects of ion implantation on surface structures and properties for bulk metallic glass, Intermetallics 17 (2009) 722–726.
[43] M. Iqbal, J.I. Akhter, Z.Q. Hu, H.F. Zhang, A. Qayyum, W.S. Sun, Mechanical properties and ion irradiation of bulk amorphous $Zr_{55}Cu_{30}Al_{10}Ni_5$ alloy, J. Non-Cryst. Solids 353 (2007) 2452–2458.
[44] E. Orowan, Symposium on Internal Stresses in Metals and Alloys, Institute of Metals, London, 1948, p. 451.
[45] L. Yang, H.Y. Li, P.W. Wang, S.Y. Wu, G.Q. Guo, B. Liao, Q.L. Guo, X.Q. Fan, P. Huang, H.B. Lou, F.M. Guo, Q.S. Zeng, T. Sun, Y. Ren, L.Y. Chen, Structural responses of metallic glasses under neutron irradiation, Sci. Rep. 7 (2017), 16739.
[46] Y. Zhang, S. Zhao, W.J. Weber, K. Nordlund, F. Granberg, F. Djurabekova, Atomic-level heterogeneity and defect dynamics in concentrated solid-solution alloys, Curr. Opin. Solid State Mater. Sci. 21 (2017) 221–237.
[47] S.J. Zinkle, L.L. Snead, Designing radiation resistance in materials for fusion energy, Annu. Rev. Mater. Res. 44 (2014) 241–267.
[48] G. Velisa, M.W. Ullah, H. Xue, K. Jin, M.L. Crespillo, H. Bei, W.J. Weber, Y. Zhang, Irradiation-induced damage evolution in concentrated Ni-based alloys, Acta Mater. 135 (2017) 54–60.
[49] M.W. Ullah, D.S. Aidhy, Y. Zhang, W.J. Weber, Damage accumulation in ion-irradiated Ni-based concentrated solid-solution alloys, Acta Mater. 109 (2016) 17–22.
[50] Z.J. Wang, C.T. Liu, P. Dou, Thermodynamics of vacancies and clusters in high-entropy alloys, Phys. Rev. Mater. 1 (2017), 043601.